Scattering and Resonances on a Quantum Simulator: From Simple Potentials to Quantum Field Theory Connections

Indrayudh Das[1, *] and Soumyadeep Sarma[1, †]

[1] *Undergraduate Programme, Indian Institute of Science, Bangalore 560012, India*

(Dated: December 1, 2025)

We present a unified study of quantum scattering and resonance phenomena for simple (0 + 1) dimensional quantum field theory, such as the double barrier and Morse potential. Using both analytical methods and numerical quantum simulations, we extract resonance lifetimes and phase shifts, relating these results to scattering definitions in quantum field theory (QFT). We further explore the feasibility of implementing such simulations on state-of-the-art IBM quantum hardware, analyzing the effects of various noise sources. Finally, we outline extensions to non-trivial potentials with exotic spectral structures.

CONTENTS

I. INTRODUCTION

The noisy-intermediate scale quantum (NISQ) era has awakened unique possibilities of realizing and studying exotic quantum many-body phases of matter and their dynamics [1], particularly in the realm of high-energy and condensed matter physics. In particular, digital quantum chips with predefined gate sets such as those accessible via Qiskit are about to enable almost anyone to run their own quantum simulations.

Within the subfield of simulations for physical systems, the study of quantum scattering and resonances has emerged as a particularly interesting application of NISQ devices. Contrary to classic solid-state realizations where scattering is often inferred from bulk transport

* indrayudhdas@iisc.ac.in
† ssoumyadeep@iisc.ac.in

properties [2], the high degree of control enables, firstly, to explore the entirety of the Hilbert space during a collision event and, secondly, to design at will and locally read out very specific dynamic quantum scattering models. For example, this opens the road to experimental information about the buildup of quantum entanglement between a scattering center and an incident wave packet [3], or the precise time-domain measurement of particle decay from a resonant trap [4].

Needless to say, gate-based quantum simulations lead to discrete time dynamics, and, therefore, their study falls under the general umbrella of digitized Hamiltonian evolution, which harbors numerical intricacies distinct from continuous analog emulation [5, 6]. Moreover, it is a nontrivial question to study when, if, and how gate errors and decoherence (noise) destroy the delicate phase information required to extract scattering phase shifts and S-matrix elements—features that are far more sensitive to dephasing than simple energy eigenvalues.

In this context, scattering and resonances are central to understanding tunneling and decay in quantum systems, acting as the fundamental probe for interaction potentials [7]. The extraction of resonance lifetimes and scattering phase shifts is of paramount importance, as these quantities encode the detailed spectroscopic information of the system, from molecular dissociation [8] to nuclear decay [9]. Quantum simulation serves as a burgeoning experimental platform for these phenomena, providing a pathway to simulate systems that are classically intractable. Furthermore, these non-relativistic studies serve as a crucial testbed, linking directly to the more complex machinery of quantum field theory (QFT) scattering amplitudes and the S-matrix [10, 11].

In this paper, we theoretically study a gate-based quantum simulation of non-relativistic quantum mechanical (NRQM) scattering for simple potentials like the double barrier and Morse potential. The paper is structured as follows. We start by summarizing the analytical formulation of scattering in the NRQM setting in Sec. II, applied to potentials considered in this work in Sec. III. We explain the quantum circuit approach used for studying scattering in Sec. IV, complementing it with a summary on noise models used in Sec. V. Results and analysis of our simulations is present in Sec. VI. We end with connecting scattering in the NRQM setting to the S-matrix formulation used in QFT in Sec. VII.

II. THEORY OF QUANTUM SCATTERING AND RESONANCES

A. General Framework

To define scattering for a non-relativistic particle we first define the state space where the state of particle lives in.

1. The Hilbert Space

The Hilbert space is defined as complex inner product which is also a metric space with respect to the distance function induced by the inner product. A single non-relativistic particle state $|\Psi\rangle \in \mathcal{H} = L^2(\mathbb{R}^3)$

2. The Hamiltonian

In scattering theory we tend to decompose the Hamiltonian into two part:

1. The free part(H_0): This consists of the kinetic part:

$$H_0 = -\frac{p^2}{2m}\nabla^2$$

2. The effective interaction potential V.

Assumption: $V(x)$ is localized, i.e $V(x) \to 0$ as $|x| \to \infty$

3. Scattering States and Lippmann–Schwinger Equation

Scattering states at energy $E = \hbar^2 k^2/2m$ satisfy

$$(H_0 + V)\left|\psi^{(\pm)}\right\rangle = E\left|\psi^{(\pm)}\right\rangle,$$

with incoming $(-)$ or outgoing $(+)$ boundary conditions. They may be written using [12] the free resolvent:

$$\left|\psi^{(\pm)}\right\rangle = |\phi_{\mathbf{k}}\rangle + \frac{1}{E - H_0 \pm i\epsilon}\, V\left|\psi^{(\pm)}\right\rangle,$$

where $|\phi_{\mathbf{k}}\rangle = e^{i\mathbf{k}\cdot\mathbf{r}}$ is the incident plane wave. In coordinate space:

$$\psi^{(+)}(\mathbf{r}) = e^{i\mathbf{k}\cdot\mathbf{r}} - \frac{m}{2\pi\hbar^2}\int d^3r'\, \frac{e^{ik|\mathbf{r}-\mathbf{r}'|}}{|\mathbf{r}-\mathbf{r}'|} V(\mathbf{r}')\psi^{(+)}(\mathbf{r}').$$

4. Asymptotic Form and Scattering Amplitude

For large r the outgoing solution takes the universal form [12]

$$\psi^{(+)}(\mathbf{r}) \xrightarrow[r\to\infty]{} e^{i\mathbf{k}\cdot\mathbf{r}} + f(\theta)\,\frac{e^{ikr}}{r},$$

where $f(\theta)$ is the scattering amplitude. The differential cross section is

$$\frac{d\sigma}{d\Omega} = |f(\theta)|^2.$$

5. Born Approximation

For weak V one substitutes the incident plane wave into the integral:

$$f^{(1)}(\theta) = -\frac{m}{2\pi\hbar^2}\int d^3r\, e^{-i\mathbf{q}\cdot\mathbf{r}}V(\mathbf{r}), \qquad \mathbf{q} = \mathbf{k}' - \mathbf{k}.$$

B. Partial Waves and Phase Shifts

For spherically symmetric $V(r)$ the wavefunction expands in partial waves:

$$\psi(r,\theta) = \sum_\ell (2\ell+1)P_\ell(\cos\theta)\, R_\ell(r).$$

The radial function satisfies

$$-\frac{\hbar^2}{2m}u_\ell'' + \left[V(r) + \frac{\hbar^2\ell(\ell+1)}{2mr^2}\right]u_\ell = Eu_\ell.$$

Its large-r behaviour defines the phase shift $\delta_\ell(k)$:

$$u_\ell(r) \sim \sin\!\left(kr - \frac{\ell\pi}{2} + \delta_\ell\right).$$

The amplitude becomes

$$f(\theta) = \frac{1}{k}\sum_\ell (2\ell+1)e^{i\delta_\ell}\sin\delta_\ell\, P_\ell(\cos\theta),$$

and the total cross section is

$$\sigma_{\rm tot} = \frac{4\pi}{k^2}\sum_\ell (2\ell+1)\sin^2\delta_\ell.$$

C. Resonances (Breit–Wigner)

A resonance occurs when a partial-wave phase shift passes through $\pi/2$ rapidly:

$$\delta_\ell(E) \approx \arctan\frac{\Gamma/2}{E - E_r}.$$

Near the resonance energy E_r,

$$\sigma_\ell(E) \simeq \frac{\pi}{k^2}(2\ell+1)\,\frac{\Gamma^2/4}{(E-E_r)^2 + \Gamma^2/4},$$

the familiar Breit–Wigner form. The width Γ relates to the lifetime τ of the quasi-bound state via $\tau \simeq \hbar/\Gamma$.

III. MODEL POTENTIALS

A. Double Barrier Potential

The double barrier potential is a prototypical model for tunneling, resonant transmission, and metastable (quasi-bound) states. It consists of two finite barriers of height V_0 separated by a well of width b. In our simulations we use the piecewise-constant form

$$V(x) = \begin{cases} V_0, & x \in [-b/2-a, -b/2)\cup[b/2, b/2+a), \\ 0, & \text{otherwise} \end{cases} \tag{1}$$

which models two rectangular barriers of width a enclosing a free region of width b. More general smooth double-barrier profiles can be used; the rectangular form provides closed expressions for scattering coefficients and is ideal for benchmarking.

1. Analytic transmission coefficient

For the piecewise-constant profile the transmission amplitude can be written in closed form without derivation. Let

$$k = \sqrt{\frac{2mE}{\hbar^2}}, \qquad \kappa = \sqrt{\frac{2m(E-V_0)}{\hbar^2}} \quad (E > V_0).$$

Define the single-barrier transmission and reflection through a region of width a:

$$t_a = \left[\cosh(\kappa a) + \frac{i}{2}\left(\frac{\kappa}{k} - \frac{k}{\kappa}\right)\sinh(\kappa a)\right]^{-1},$$

$$r_a = \frac{i}{2}\left(\frac{\kappa}{k} + \frac{k}{\kappa}\right)\sinh(\kappa a)\; t_a.$$

Propagation across the intermediate well of width b contributes only the phase factor e^{ikb}.

The full transmission amplitude of the double barrier is

$$t(E) = \frac{t_a^2\, e^{ikb}}{1 - r_a^2\, e^{2ikb}} = |t(E)|e^{i\phi(E)}. \tag{2}$$

where $E = k^2$ (we take $2m = 1$ throughout). This phase $\phi(E) \equiv 2\delta(E)$ The corresponding transmission probability is

$$T(E) = |t(E)|^2 = \frac{|t_a|^4}{|1 - r_a^2 e^{2ikb}|^2}.$$

The resonance condition occurs when the denominator in (2) nearly vanishes,

$$|1 - r_a^2 e^{2ikb}| \approx 0,$$

or equivalently when

$$2kb + 2\arg(r_a) = 2\pi n, \qquad n \in \mathbb{Z}.$$

This selects energies close to quasi-bound states in the interior well.

2. Resonances and lifetime

Resonances occur when the denominator in (2) is small,

$$1 - r_a^2 e^{2ikb} \approx 0.$$

Write $r_a = |r_a| e^{i\varphi_r}$ and define the phase function

$$\theta(E) := k(E)\, b + \varphi_r(E), \qquad k(E) = \sqrt{2mE}/\hbar.$$

The resonance *energy* E_R is determined by the phase condition

$$2\theta(E_R) = 2\pi n \quad \Longleftrightarrow \quad k_R b + \varphi_r(E_R) = \pi n, \tag{3}$$

with $k_R \equiv k(E_R)$ and $n \in \mathbb{Z}$.

To obtain the resonance *width* we linearize the denominator near E_R. Set $\rho := |r_a|^2$ (< 1) and expand

$$1 - \rho e^{2i\theta(E)} \simeq (1-\rho) - 2i\rho\, \theta'(E_R)\,(E - E_R),$$

where $\theta'(E_R) = \frac{d\theta}{dE}\big|_{E_R}$. Using

$$\frac{dk}{dE} = \frac{m}{\hbar^2 k}, \qquad \theta'(E_R) = \frac{mb}{\hbar^2 k_R} + \left.\frac{d\varphi_r}{dE}\right|_{E_R},$$

the transmission probability near E_R takes the Breit–Wigner form

$$|t(E)|^2 \approx \mathcal{A} \frac{\Gamma/2}{(E - E_R)^2 + (\Gamma/2)^2},$$

with the resonance width

$$\boxed{\Gamma \;=\; \frac{1-\rho}{\rho\, \theta'(E_R)} \;=\; \frac{1 - |r_a|^2}{|r_a|^2 \left(\frac{mb}{\hbar^2 k_R} + \frac{d\varphi_r}{dE}\right)_{E_R}}.} \tag{4}$$

$$\varphi_r(E) = \arctan\left(\frac{\coth \kappa a}{\alpha(E)}\right), \; \alpha(E) = \frac{\kappa^2 - k^2}{2k\kappa} \tag{5}$$

The prefactor $\mathcal{A}$ depends on the numerator $t_a^2 e^{ikb}$ evaluated at E_R; importantly the lifetime is

$$\tau \;=\; \frac{\hbar}{\Gamma}.$$

These resonances arise purely from quantum interference between repeated reflections inside the central well.

B. Morse Potential

The Morse potential [13] is a one-dimensional, exactly solvable model widely used for anharmonic vibrational motion of diatomic molecules. We adopt the common form

$$V(x) = D\big(e^{-2a(x-x_0)} - 2e^{-a(x-x_0)}\big), \quad x > 0 \tag{6}$$

with depth parameter $D > 0$, range parameter $a > 0$ (inverse length), and equilibrium position x_0. This form has a minimum $V(x_0) = -D$ and approaches zero as $x \to +\infty$.

Introduce the dimensionless coordinate $y = a(x - x_0)$ and the parameter

$$\nu = \frac{\sqrt{2mD}}{\hbar a},$$

and measure energies relative to the continuum threshold ($E = 0$ at $x \to +\infty$).

1. Bound states: energies and wavefunctions

The potential supports a finite number of bound states. The exact bound-state energies (measured from the continuum at $E = 0$) are

$$E_n = -\frac{\hbar^2 a^2}{2m}\big(\nu - n - \tfrac{1}{2}\big)^2, \qquad n = 0, 1, \ldots, n_{\max}, \tag{7}$$

with the quantization condition $\nu - n - \frac{1}{2} > 0$. Thus the number of bound states is

$$n_{\max} + 1 = \big\lfloor \nu + \tfrac{1}{2} \big\rfloor.$$

Defining $\xi = 2\nu e^{-y} = 2\nu e^{-a(x-x_0)}$ and $s_n = \nu - n - \frac{1}{2}$, the normalized bound eigenfunctions are

$$\psi_n(x) = \mathcal{N}_n\, \xi^{s_n}\, e^{-\xi/2}\, L_n^{(2s_n)}(\xi), \tag{8}$$

where $L_n^{(\alpha)}(\xi)$ are associated Laguerre polynomials and

$$\mathcal{N}_n = \sqrt{\frac{a\, n!}{\Gamma(2s_n + n + 1)}}.$$

2. Scattering states and the S–matrix

For continuum energies $E > 0$ the scattering solutions can be expressed in terms of confluent hypergeometric (Whittaker) functions [14]. The one-dimensional elastic S–matrix (phase shift $\delta(k)$ defined by $\psi_k(x) \sim e^{ikx} + e^{2i\delta(k)} e^{-ikx}$ as $x \to +\infty$) admits a compact representation in terms of Gamma functions:

$$S(k) = e^{2i\delta(k)} = \frac{\Gamma(1 + 2i\kappa)}{\Gamma(1 - 2i\kappa)} \cdot \frac{\Gamma(\frac{1}{2} - \nu - i\kappa)}{\Gamma(\frac{1}{2} - \nu + i\kappa)},$$

where $\kappa = k/a$ is the dimensionless momentum. Poles of the analytically continued $S(k)$ on the positive imaginary axis correspond to the bound states (7).

Although the Morse potential lacks an internal barrier that would produce sharp shape resonances like a double-barrier system, rapid variation of the phase shift can occur near threshold when weakly bound states approach dissociation; this behaviour can mimic resonance-like scattering in near-dissociation spectroscopy.

IV. QUANTUM SIMULATION APPROACH

A. Approaches to encoding

While there are many frameworks and bases for encoding states, we utilize JLP encoding [], which we have used for NRQM. For a general field ϕ, we discretize it over a grid of $N = 2^{n_q}$ points (n qubits) in the range $[-\phi_{\max}, \phi_{\max})$. Then we have $\Delta\phi = 2\phi_{\max}/N$ and $\phi_m = m\Delta\phi$, with m ranging from $-N/2$ to $N/2-1$ in steps of 1. For the Hamiltonian $\mathcal{H}(\hat{\phi}, \hat{\Pi})$, we have the field basis:

$$\hat{\phi}\,|\phi_m\rangle = \phi_m\,|\phi_m\rangle\,.$$

For the momentum grid, we have $p_m = m\pi/\Delta\phi$, using which we have the direct Fourier transform (DFT):

$$F_{mj} = \frac{1}{\sqrt{N}} e^{i\Pi_m \phi_j},$$

with both indices going from $-N/2$ to $N/2-1$. The conjugate momentum operator $\hat{\Pi}$ becomes:

$$\hat{\Pi} = F^\dagger \mathrm{diag}(\Pi_m) F.$$

An advantage of utilizing this encoding is that the potential becomes a diagonal matrix $V = \mathrm{diag}(V(\phi_m))$. However, implementing such gates exactly with a gate decomposition into primitive one and two-qubit gates is very difficult. We have directly used Qiskit's `DiagonalGate` to simulate the unitary $U_V = e^{-iV\Delta t}$. We mention in passing that for a double-barrier potential, quantum modular arithmetic, used to compare bitstrings with quantum adders and subtractors, is a promising, albeit high-depth ($\mathcal{O}(2^{n_q})$ CNOT gates), implementation of the potential. Finally, the $\hat{\Pi}$ in momentum basis is:

$$\hat{\Pi} = -\frac{\pi}{N\Delta\phi} \sum_{l=0}^{n_q-1} 2^l Z_l$$

Hence, the $\hat{\Pi}^2$ gate decomposition is just $R_{ZZ}(\theta) = e^{-i\theta Z_i Z_j}$ gates sandwiched between two QFT gates.

B. Trotterized Hamiltonian Evolution

The general Hamiltonian type considered in this term paper is of the form of a kinetic interaction $\mathcal{H}_{\text{kin}} = \hat{\Pi}^2/2$ and interacting terms $\mathcal{H}_{\text{int}} = V(\hat{\phi})$. We consider the position and momentum scalar fields $\hat{\phi} \equiv \hat{x}$, $\hat{\Pi} \equiv \hat{p}$. For a general step-wise unitary evolution $U_{\Delta t} = e^{-i\mathcal{H}\Delta t} = e^{\lambda(\mathcal{H}_{\text{kin}}+\mathcal{H}_{\text{int}})}$, the general $k-$th order Suzuki-trotter expansion is:

$$S_{2k}(\lambda) = S_{2k-2}(s_{2k}\lambda)^2 S_{2k-2}((1-4s_{2k})\lambda)) S_{2k-2}(s_{2k}\lambda)^2,$$
$$4s_{2k}^{2k-1} + (1-4s_{2k})^{2k-1} = 0. \tag{9}$$

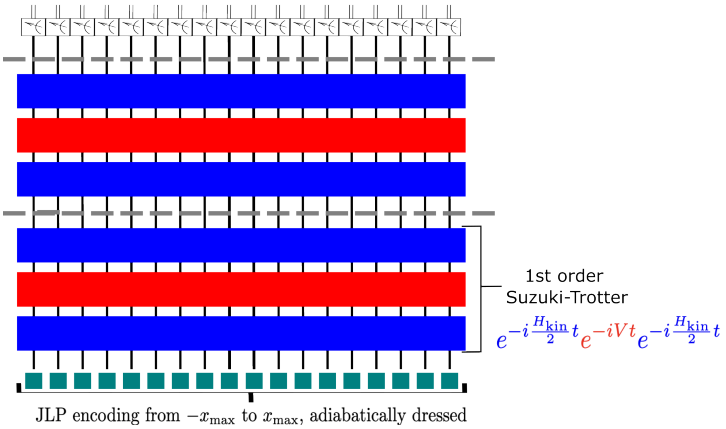

FIG. 1. Quantum circuit diagram utilized for NRQM simulations.

The error here is $\mathcal{O}((\Delta t)^{2k+1})$ and $k=1$ is the Strang order formulation $e^{\lambda(\mathcal{H}_{\text{kin}}+\mathcal{H}_{\text{int}})} = e^{\lambda\mathcal{H}_{\text{kin}}/2} e^{\lambda\mathcal{H}_{\text{int}}} e^{\lambda\mathcal{H}_{\text{kin}}/2} + \mathcal{O}((\Delta t)^3)$. The Lie-Trotter approximation is taken as $e^{\lambda\mathcal{H}_{\text{kin}}} e^{\lambda\mathcal{H}_{\text{int}}} + \mathcal{O}((\Delta t)^2)$.

C. Algorithmic Implementation

This subsection presents the quantum circuit approach used for our simulations.

The first step is *adiabatic state preparation*. The idea derives from the adiabatic theorem in quantum mechanics [15], which says that for a finite, non-degenerate spectrum with a finite gap between any pair of eigenstates over a slowly varying Hamiltonian, we can start off with a ground state of the $\mathcal{H}_{\text{kin}}$ (will be plane waves in our case) created in the momentum-basis as a one-particle state localized at $-x_0$ with the momentum centralized around $\mp k_0$:

$$|\psi_{\text{free}}\rangle\,(0) = \left(\sum_{k_1} g_{-x_0}(k_1) a^\dagger_{k_1}\right)|0\rangle\,.$$

Here, the bracket in the LHS corresponds to the time-evolution variable. $|0\rangle$ is the vacuum state (no particles added) with:

$$g_{-x_0}(k) \sim e^{-ikx_0} e^{-\frac{(k-k_0)^2}{2\sigma_k}}.$$

For implementation, we have used a simplified version for creating a moving Gaussian packet in the position basis, given as:

$$|\psi_{\text{free}}\rangle = N \sum_l e^{ik_0(x_m - x_0)} e^{-\frac{(x_m-x_0)^2}{2\sigma_x}}\,|x_m\rangle\,,$$

where N is the normalization and $\{|x_m\rangle \equiv |m_{(2)}\rangle\}$ are the JLP basis states ($\hat{\phi}$ in IV A is taken as $\hat{x}$ here.)

Here, σ_x is chosen so as to ensure that the wave-packet is sharply localized at $-x_0$. We then evolve the $|\psi\rangle_{\text{free}}$

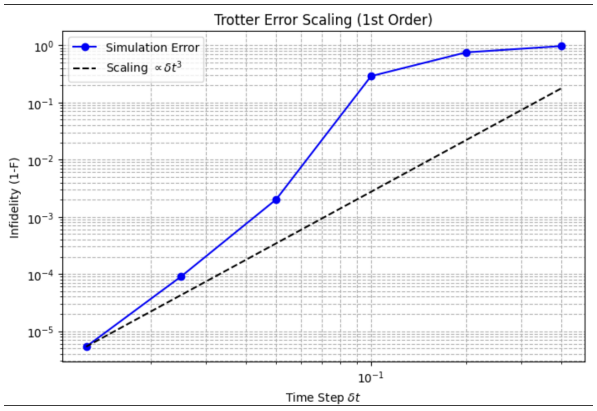

FIG. 2. Log-log plot of infidelity (1 - fidelity) versus Δt for double barrier potential with $n_q = 5$ qubits.

with $\mathcal{H}(s) = \mathcal{H}_{\text{kin}} + r(s)\mathcal{H}_{\text{int}}$, with a smooth adiabatic ramp $r(s)$, with $s = t/T \in [0,1] \mapsto r(s) \in [0,1]$. We choose a boundary-flattened ramp to keep leakage as $\mathcal{O}(1/T^2)$ and utilize states in the intended $\mathbb{Z}_2$ parity-conserved sector. This gives us $|\psi_{\text{int}}\rangle(0)$

Next, we involve a time-evolution via a first-order Suzuki-Trotter evolution, with N_s steps over a time-evolution T_s, making $\Delta t = T_s/N_s$, and $U(T_s) = (S_2(\Delta t))^{N_s}$ [cf. Fig. 1]. Higher orders may be considered, optimizing the competing forces of higher gate-count error with smaller errors from higher-order (Δt). We have benchmarked our Trotter error against exact diagonalization (ED) in Fig. 2 to obtain the expected $\mathcal{O}((\Delta t)^3)$ error scaling.

After the evolution, we get $|\psi_{\text{int}}\rangle(T_s) = U(T_s)|\psi_{\text{int}}\rangle(0)$. We have two ways of extracting phase shift information from our scattered wavepacket:

1. We compute the overlap with a free evolution to get the overlap function $C(\Delta T) = \langle\psi_{\text{free}}(T_s + \Delta T)|\psi_{\text{int}}(T_s)\rangle$. The peak of this yields $\tau(k_0) = 2(d\delta/dk)|_{k_0}$ which integrates locally to $\delta(k_0)$.

2. From analytics, we know the form of the wave packet carrying the phase shift ($\sim S(k)e^{\pm ikx}$ for the double barrier and Morse potential, respectively, see Sec. III). We overlap with that wave packet by explicitly choosing the sign of momentum in the momentum-basis representation and "masking" (i.e., putting to zero) the amplitudes of other momenta. Dividing the amplitude arrays for the phase-shifted and free parts gives us $S(k) = e^{2i\delta(k)}$ for a range of k used in the wave packet. In the double-barrier potential, this division of amplitude arrays in momentum space can also give $t(k)$ and $r(k)$.

We have utilised the second method. Here we remark that the overlap $\langle\psi_{\text{free}}|\psi_{\text{int}}|\psi_{\text{free}}|\psi_{\text{int}}\rangle$ can be done using a Hadamard test [16]. For numerical accuracy in the noiseless simulations, we have instead utilized Qiskit's `Statevector` simulations and directly compared the NumPy arrays to obtain phase shifts, transmission and reflection coefficients, etc.

V. NOISE MODELLING AND ERROR MITIGATION

As a deep dive, we have conducted noise modeling in addition to noiseless simulations. This section summarizes the noise models employed in our simulations. We utilize a quantum noise channel in an operator-sum formalism on our state density matrix ρ [] such that $\varepsilon(\rho) = \sum_k E_k \rho E_k^\dagger$, with our error operators including a factor $\sqrt{p_k}$, where p_k is the probability of error E_k happening.

Depolarizing noise: This corresponds to a qubit going to a maximally mixed state $I/2$ with probability p. The quantum channel is described as:

$$\varepsilon(\rho) = (1-p)\rho + \frac{p}{3}(X\rho X + Y\rho Y + Z\rho Z).$$

This can easily be generalized to more than one qubit. In Qiskit, we have used `Qiskit_aer` noise models containing a depolarizing error model which adds a single-qubit X, Y, Z error gate with probability $p_1/3$ after every single-qubit in the quantum circuit. Two-qubit gates utilize $p_2 \approx 10p_1$, as observed in state-of-the-art hardware.

Decoherence: This model essentially employs two quantum noise channels of Amplitude Damping and Phase Damping simultaneously. In amplitude damping:

$$E_0 = \begin{bmatrix} 1 & 0 \\ 0 & \sqrt{1-\gamma_1} \end{bmatrix}, \; E_1 = \begin{bmatrix} 0 & \sqrt{\gamma_1} \\ 0 & 0 \end{bmatrix}, \; \gamma_1 = 1 - e^{t/T_1},$$

includes converting $|1\rangle$ to $|0\rangle$ and reducing amplitude of $|1\rangle$, while phase damping:

$$E_0 = \begin{bmatrix} 1 & 0 \\ 0 & \sqrt{1-\gamma_2} \end{bmatrix}, \; E_1 = \begin{bmatrix} 0 & 0 \\ 0 & \sqrt{\gamma_2} \end{bmatrix}, \; \gamma_2 = 1 - e^{t/T_2}$$

destroys the $|0\rangle$ state.

Another commonly seen error is the state preparation and measurement (SPAM) error, where the classically measured probabilities are skewed due to a confusion matrix. In practice, mitigating this error is much easier, as it involves finding the confusion matrix empirically and then applying the inverted confusion matrix to the final probability counts obtained from the simulation. Hence, we have only considered decoherence and depolarizing noise channels.

Mitigating errors: For decoherence, dynamical decoupling to apply π pulses on idle gates extends the effective T_2 time. Other methods involve optimized transpilation to reduce the number of CNOTs, zero-noise extrapolation to obtain measurements in the zero-noise limit extrapolated from noise-amplified runs, randomized coupling and symmetrization to convert coherent over-rotation errors to stochastic noise and average them out over a long run.

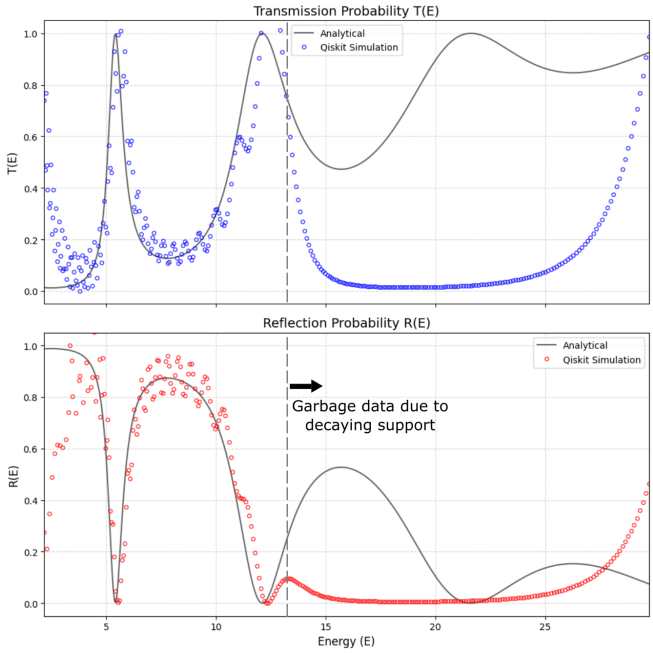

FIG. 3. Transmission and reflection probabilities as a function of energy for $V_0 = 4, b = 0.5, w = 2, n_q = 12$. The wave packet used has energy centered around $E_0 = 10$ with $\sigma_x = 1.0$.

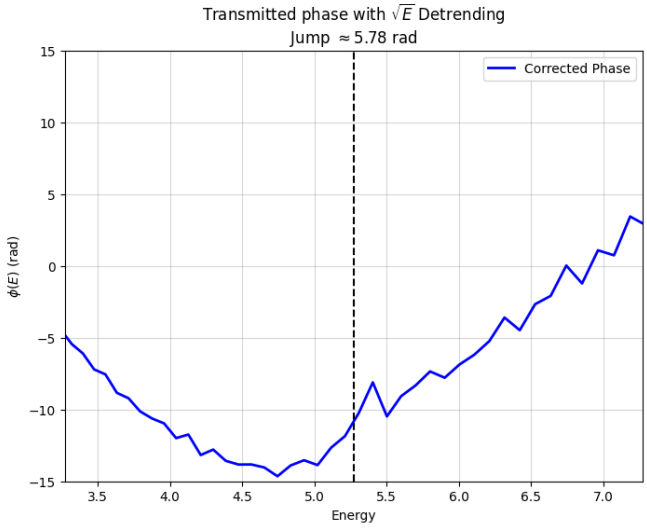

FIG. 4. Phase shift $\phi(E)$ jumps approximately by π radians across the resonance $E_r \approx 5.35$. Simulation parameters same as used in Fig. 3

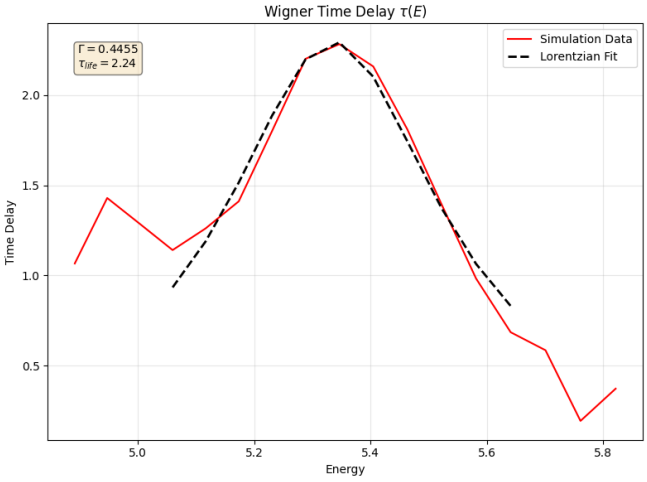

FIG. 5. Time delay across resonance obtained using NumPy gradient across the transmission phase plot, including the background phase ($\phi(E)$ from Fig. 4 + $\mathcal{O}(\sqrt{E})$ corrections). A Lorentzian fit at the resonance energy gives $\Gamma = 0.445 \implies \tau_l = 2.2$ (in units of Δt). Simulation parameters same as used in Fig. 3.

VI. RESULTS AND ANALYSIS

A. Resonance Features in the Double Barrier

As shown in Sec. IV C, we obtain transmission ($T(E) = |t(E)|^2$) and reflection ($R(E) = |r(E)|^2$) probabilities by dividing the masked out transmitted and reflected wavepacket amplitudes with the free evolution amplitudes in the momentum space. The results for one such analysis is highlighted in Fig. 3.

One point to highlight is the data points flocking around 0 for both $T(E)$ and $R(E)$ after $E > 12$ in Fig. 3. In the code, we have used a parameter $\epsilon = 10^{-12}$ to avoid division by zero:

$$T(k) = |c_T(k)|^2/|c(k) + \epsilon|^2,$$
$$R(k) = |c_R(k)|^2/|c(k) + \epsilon|^2,$$

where $|\psi_{\text{free}}\rangle = \sum c(k)\,|k\rangle\,,\ |\psi_{T,R}\rangle = \sum c_{T,R}(k)\,|k\rangle$. Due to the wave packet having less support (i.e. very small amplitudes $c_{T,R}(k)$) at higher energies, our fraction gets dominated by ϵ, and hence goes to 0. We obtain the phase $\phi(E)$ from $t(E)$, and check around the resonance energy $E_r \approx 5.35$ to obtain the phase jump as seen in Fig. 4 after doing a $\sqrt{E}$ detrending of the background phase e^{ikb} [cf. Eq. 2]. Previously, we were performing a linear de-trending, which did not accurately highlight the jump (as seen in the presentation!).

By utilizing a NumPy gradient method, I obtained the time delay around the resonance peak as $\tau(E) = 2d\delta/dE = d\phi/dE$, and curve-fitted a Lorentzian function to determine the decay width Γ and thus the resonance lifetime $\tau_l = \hbar/\Gamma$, as shown in Fig. 5.

B. Resonances in the Morse Potential

Similarly, we computed the total phase shift for the Morse potential as a function of energy. In the case of the double-barrier potential, sending a single wavepacket centered around E_0 did not provide sufficient support to accurately extract the total phase. To obtain

smoother and more reliable data, we instead used multiple wavepackets uniformly distributed across the energy domain.

Furthermore, this simulation employs the Log-Derivative method, which is known to stabilize solutions for long-ranged potentials. The resulting phase-shift curve is shown in Fig. 6. In Fig. 7, we plot the time delay as a function of energy, which exhibits a clear resonance peak at $\sqrt{E} = 1.36\,\mathrm{fm}^{-1}$ with a decay width $\Gamma = 0.0268\,\mathrm{fm}^{-1}$.

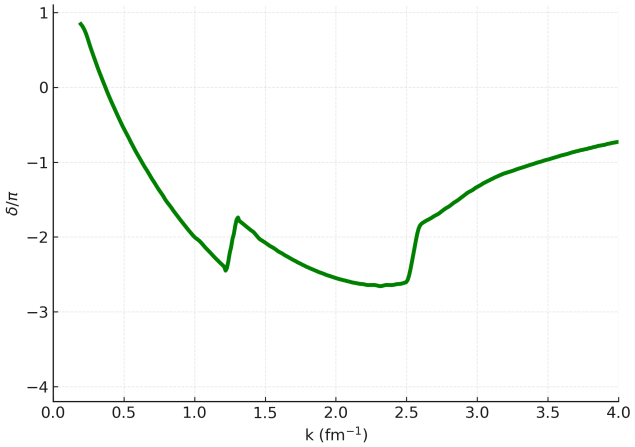

FIG. 6. Phase shift $\delta(E)$ again jumps approximately by π radians at $\sqrt{E_R} = 1.36957$ fm^{-1}. Simulation parameters used are $D = 6$ fm^{-2}

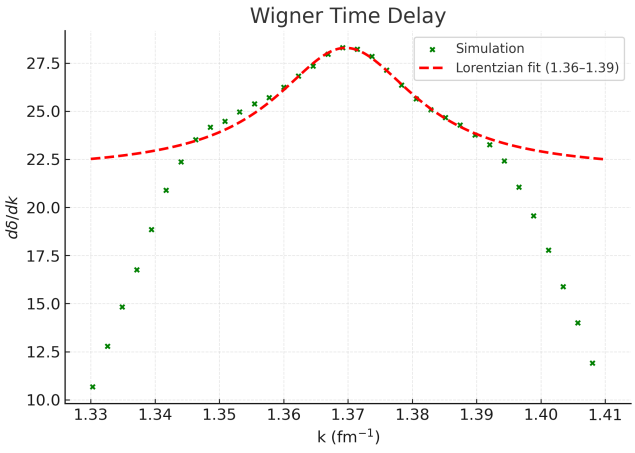

FIG. 7. Lorentzian fit around $\sqrt{E_R} = 1.36957 fm^{-1}$ gives: $\Gamma = 0.026898$ $fm^{-1} \implies \tau = 37.17$ fs

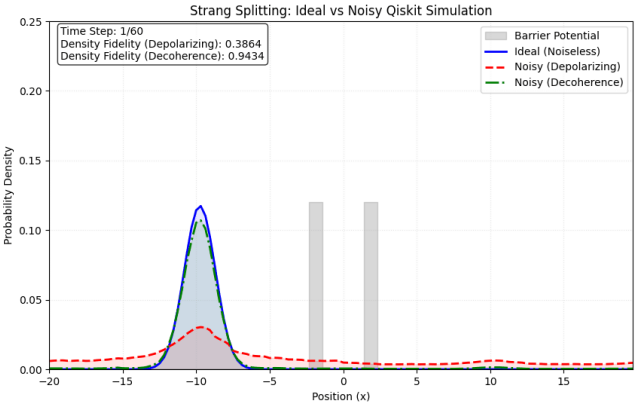

FIG. 8. Noiseless simulation (blue) overlayed on top of simulation with depoloarizing noise (red) for double barrier potential just after simulation start, with $p_1, p_2 = 5\times10^{-4}, 5\times10^{-3}$ and decoherence times of $T_1, T_2 = 90\mu s, 80\mu s$ with a gate time of 50 ns. Qiskit Aer's density matrix simulation utilized. Potential parameters: $V_0 = 4, a = 1, b = 2.5$ [cf. Eq. 1]. Simulation parameters $E_0 = 9,\ \sigma_x = 1.5, n_q = 7$.

C. Extracted Lifetimes and Uncertainties

D. Noisy simulation results

As highlighted in Sec. V, we have utilised depolarizing and decoherence noise models from Qiskit's `NoiseModel` class. Figs. 8 and 9 presents snapshots of these noisy simulation results just after the simulation is started for double barrier and Morse potentials respectively. It is clear the even with the lowest possible state-of-the-art error rates, both types of noise simply convert the system to a maximally mixed state (completely constant probability distribution), with depolarizing noise affecting the simulations much more.

A possible explanation is in the number of entangling gates in the circuit. Assuming a perfect diagonal potential gate implementation, we have initialized two-qubit gates error to only depolarizing noise (with probability $p_2 \approx 10p_1$, where p_1 is single gate error probability) in our simulations to isolate its effects. The QFT gate used in the circuit has $\mathcal{O}(n_q^2)$ number of CNOT gates, and hence results in a very fast propagation of error every trotter step as compared to single-qubit gate decoherence error propagation.

E. Circuit entanglement results

Another interesting observable is bipartite von Neumann entanglement entropy of the state as a function of trotter steps. Figs. 10 and 11 highlight the same for simulations in double barrier and More potentials. Some key things to unpack here are:

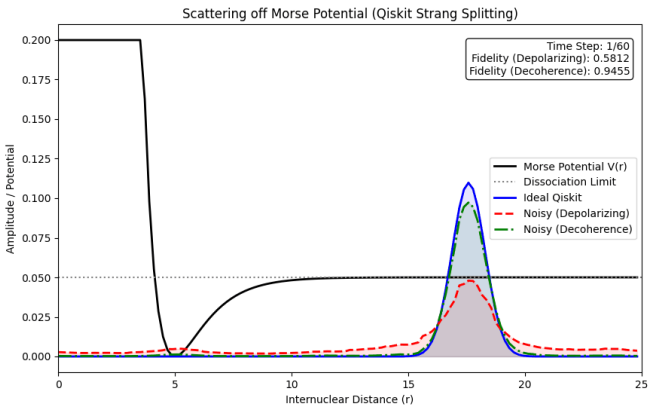

FIG. 9. Noiseless simulation (blue) overlayed on top of simulation with depolarizing noise (red) for Morse potential just after simulation start, with potential parameters: $D = 20$, $a = 8$, $x_0 = 5.0$ [cf. Eq. 6]. All other noise and simulation parameters same as used in Fig. 8.

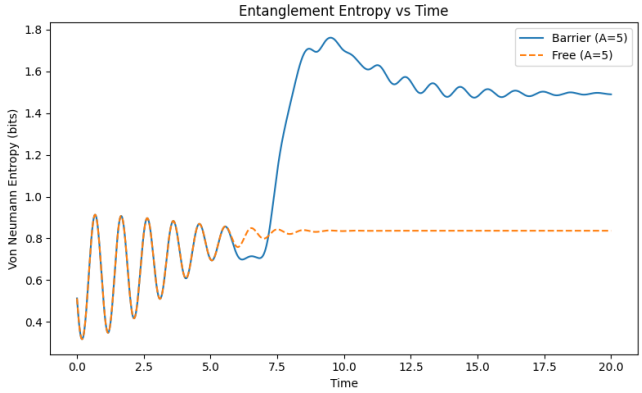

FIG. 10. Entanglement entropy of the wavepacket in Double barrier potential(blue) and Free potential(orange). Parameters used h(barrier height) $= 5$, w(width) $= 11$ with 10 qubits

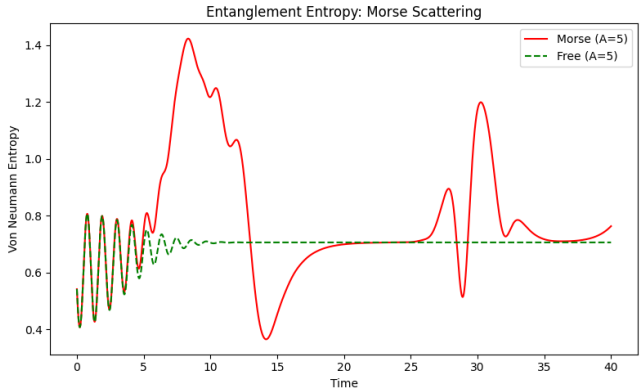

FIG. 11. Entanglement entropy of the wavepacket in Morse potential(red) and Free potential(green). Parameters used $D = 5$, $\alpha = 0.12$ with 10 qubits

- The decaying oscillating behaviour of the free wave packet comes from two factors: phase coherence at $x = 0$ boundary and dispersion of the packet. The phase factor obtained from summing over $e^{-iE_k t}$, $E_k \sim k^2$ at the partition boundary (let's say $x = d$) controls the coherences of the reduced density matrix in the form of correlator functions of the form $\int_{x<d} \mathrm{d}x \int_{y>d} \mathrm{d}y\ \psi^*(x)\psi(y)$. Since the faster moving waves reach at $x = 0$ first, the contribution of the phases goes decreasing in k, highlighting the slight dip in frequency. The decay is attributed to the Gaussian envelope width $\sigma(t)$ spreading with time, and thus lowering the magnitude of $|\psi(0,t)|^2$.

- In double barrier simulation [cf. Fig. 10], a clear jump is observed after the scattering at $t \approx 7.5$. This is intuitively understood as forming a sort of Bell-state with very high entanglement after the scattering as the wave-packet separates out into transmitted ($|\psi_T\rangle$ with most support at $x > 0$) and reflected ($|\psi_R\rangle$ with most support at $x < 0$) parts, $|\psi_{\text{int}}\rangle \approx |0\rangle |\psi_R\rangle + |1\rangle |\psi_T\rangle$. Here the first qubit is the most significant bit (MSB) in the JLP basis, highlighting if the wavepacket is at $x < 0$ ($|0\rangle$) or $x > 1$ ($|1\rangle$).

- For Morse potential simulation [cf. Fig. 11], we use hard wall interaction at the right end of the simulation frame. We observe the entropy to stabilize to the free evolution value after the jump introduced by the scattering potential at $t \approx 5$ due to decay introduced by the wave packet dispersion, after which it collides with the hard wall at around $t \approx 25$.

VII. CONNECTION TO SCATTERING IN QUANTUM FIELD THEORY

A. General Framework of Scattering

1. *Evolution operators*

- The free evolution operator(U_0): $U_0 = e^{-iH_0 t}$
- The full evolution operator(U): $U = e^{-iHt}$

To evolve a state from initial state to time at t: $|\psi(t)\rangle = U(t)|\psi(0)\rangle$

2. *Asymptotic States and Wave operators*

We define Møller wave operators [17] $\Omega_\pm$:

$$\Omega_\pm = \lim_{t \to \mp} U^\dagger(t) U_0(t)$$

With the above stated assumptions one can prove that the limit exists.

3. The Scattering operator

The primary goal of scattering theory is to determine how an initial free state ("in-state") evolves into a final free state ("out-state") after the interaction. The scattering or S matrix [18] is defined as:

$$S = \Omega_-^\dagger \Omega_+$$

With this definition an asymptotic state $|\psi\rangle_{\text{in}}$ is related to $|\psi\rangle_{\text{out}}$ by [19]:

$$|\psi\rangle_{\text{out}} = S|\psi\rangle_{\text{in}}$$

4. Asymptotic states

Let $|\psi\rangle \in \mathcal{H}$ be a state in the Hilbert space at time $t = 0$. This $|\psi\rangle$ is our physical or interacting state.
We say that ψ is a scattering state if it satisfies the asymptotic condition, which means there exist two free states, ϕ_{in} and ϕ_{out}, such that:

- Asymptotic "In" State (ϕ_{in}): The state ψ is said to have an asymptotic in-state ϕ_{in} if the actual evolved state $U(t)\psi$ becomes indistinguishable from the freely evolved state $U_0(t)\phi_{in}$ in the distant past.

$$\lim_{t\to-\infty} \|U(t)\psi - U_0(t)\phi_{in}\| = 0$$

- Asymptotic "Out" State (ϕ_{out}): The state ψ is said to have an asymptotic out-state ϕ_{out} if the actual evolved state $U(t)\psi$ becomes indistinguishable from the freely evolved state $U_0(t)\phi_{out}$ in the distant future.

$$\lim_{t\to+\infty} \|U(t)\psi - U_0(t)\phi_{out}\| = 0$$

This definition is the fundamental basis for the Møller wave operators ($\Omega_\pm$) we saw earlier. The Møller operators are precisely the mathematical objects that map the asymptotic free states (ϕ_{in}, ϕ_{out}) to the physical state (ψ) at $t = 0$. By manipulating the limits in the asymptotic condition, we can find the explicit relationship:

- From the "In" State:The condition $\lim_{t\to-\infty} \|U(t)\psi - U_0(t)\phi_{in}\| = 0$ is equivalent to:

$$\psi = \left(\lim_{t\to-\infty} U(t)^\dagger U_0(t)\right)\phi_{in}$$

  This defines the Møller operator Ω_+:

$$\psi = \Omega_+\phi_{in}$$

- From the "In" State:The condition $\lim_{t\to-\infty} \|U(t)\psi - U_0(t)\phi_{in}\| = 0$ is equivalent to:

$$\psi = \left(\lim_{t\to-\infty} U(t)^\dagger U_0(t)\right)\phi_{in}$$

This defines the Møller operator Ω_+:

$$\psi = \Omega_+\phi_{in}$$

From the "Out" State:The condition $\lim_{t\to+\infty} \|U(t)\psi - U_0(t)\phi_{out}\| = 0$ is equivalent to:

$$\psi = \left(\lim_{t\to+\infty} U(t)^\dagger U_0(t)\right)\phi_{out}$$

This defines the Møller operator Ω_-:

$$\psi = \Omega_-\phi_{out}$$

B. Asymptotic Dynamics in Relativistic QFT

Let $\Phi(x)$ be a scalar quantum field acting on a Hilbert space $\mathcal{H}$ that satisfies the Wightman axioms: locality, relativistic covariance, spectrum condition, and uniqueness of the vacuum. Denote by $P^\mu = (H, \mathbf{P})$ the generators of translations, with joint spectrum contained in the forward light cone.

Single-particle states lie on the isolated mass shell

$$p^\mu p_\mu = m^2, \qquad p^0 > 0,$$

with inner product

$$\langle \mathbf{p}'|\mathbf{p}\rangle = 2E_{\mathbf{p}}(2\pi)^3\delta^{(3)}(\mathbf{p}-\mathbf{p}'), \qquad E_{\mathbf{p}} = \sqrt{\mathbf{p}^2 + m^2}.$$

As in non-relativistic scattering, we decompose the Hamiltonian as

$$H = H_0 + V,$$

where H_0 is the free relativistic Hamiltonian and V contains the interactions.

The Møller operators are defined formally by the strong limits

$$\Omega_\pm = \lim_{t\to\mp\infty} e^{+iHt}e^{-iH_0t},$$

whenever these limits exist. Under a mass gap assumption, the existence of these limits and their basic properties follow from the Haag–Ruelle theorem. The scattering operator is then

$$S = \Omega_-^\dagger\Omega_+.$$

C. Non-Relativistic Potential Scattering as a 0+1 Dimensional QFT

The Schrödinger Hamiltonian

$$H = \frac{p^2}{2m} + V(x)$$

describes the dynamics of the one–particle sector of a 0+1-dimensional quantum field theory with field operator

$\phi(x)$. A Schrödinger wavefunction may be identified with a one–particle Fock state:

$$|\psi\rangle = \int dx\, \psi(x)\, a_x^\dagger |0\rangle.$$

Asymptotically, the scattering solution behaves as

$$\psi(x) \sim e^{ikx} + e^{2i\delta(k)} e^{-ikx},$$

leading to the same definition of the S–matrix,

$$S(k) = e^{2i\delta(k)}.$$

Thus the phase shifts extracted in our numerical simulation correspond exactly to the relativistic phase shifts appearing in the partial wave expansion of QFT scattering amplitudes.

D. LSZ and the Relativistic S-Matrix

The relativistic scattering amplitudes are obtained via the Lehmann–Symanzik–Zimmermann (LSZ) reduction formula [20]:

$$\langle p_1', \ldots, p_m' | S | p_1, \ldots, p_n \rangle = \left(\prod_i Z^{-1/2} \right)$$
$$\times \int \prod_j d^4x_j\, e^{ip_j \cdot x_j} (\Box_{x_j} + m^2) \langle 0 | T\Phi(x_1) \cdots \Phi(x_{n+m}) | 0 \rangle,$$

where Z is the wavefunction renormalization constant.

For elastic $2 \to 2$ scattering in one spatial dimension,

$$\mathcal{M}(s) = \frac{1}{2ik} \left(e^{2i\delta(k)} - 1 \right), \qquad s = 4(k^2 + m^2),$$

hence the non-relativistic phase shift yields the relativistic invariant amplitude through

$$\delta(k) = \frac{1}{2i} \ln(1 + 2ik\, \mathcal{M}(s)).$$

E. Resonances and Pole Structure

Resonances correspond to poles of analytically continued Green's functions or of the S–matrix.

NRQM: Resonances appear as poles of the Green's function at

$$E = E_R - i\frac{\Gamma}{2}, \qquad \Gamma = 1/\tau.$$

QFT: The Källén–Lehmann spectral representation

$$\langle 0 | T\Phi(x)\Phi(0) | 0 \rangle = \int_0^\infty d\mu^2\, \rho(\mu^2)\, \Delta_F(x; \mu^2)$$

contains a Breit–Wigner peak when an unstable particle is present,

$$\rho(\mu^2) \sim \frac{1}{(\mu^2 - m_R^2)^2 + m_R^2 \Gamma^2}.$$

In both theories,

$$S(E) \sim \frac{1}{E - (E_R - i\Gamma/2)},$$

and the lifetime τ extracted from our simulation corresponds precisely to the QFT decay width.

F. Haag–Ruelle Construction of Asymptotic States

We summarize the rigorous Haag–Ruelle construction of incoming and outgoing multi-particle states in massive relativistic QFT [21].

1. Assumptions

We assume:

1. The Wightman axioms.
2. Spectrum condition: $\mathrm{spec}(P^\mu) \subset \overline{V_+}$.
3. Unique vacuum Ω.
4. Locality.
5. A mass gap: an isolated mass shell $p^2 = m^2$ separated from the rest of $\mathrm{spec}(H)$.

Let $\mathcal{H}_1$ denote the single-particle subspace corresponding to the mass shell.

2. Haag–Ruelle Operators

Let $\Phi(x)$ be a local field, and let $f(\mathbf{x})$ be a Schwartz test function whose Fourier transform is supported near a point on the mass shell. Define

$$\Phi(f, t) = \int d^dx\, f(\mathbf{x})\, \Phi(t, \mathbf{x}).$$

Define the Haag–Ruelle creation operator

$$A(t) := \Phi(f, t)\, e^{i\omega t}, \qquad \omega(\mathbf{p}) = \sqrt{\mathbf{p}^2 + m^2}.$$

Given n wavepackets f_i with mutually disjoint velocity supports, define

$$\Psi_t := A_1(t) A_2(t) \cdots A_n(t)\, \Omega.$$

[Haag–Ruelle] Under the assumptions above and disjoint velocity supports, the limits

$$\Psi_{\mathrm{out}} = \lim_{t \to +\infty} \Psi_t, \qquad \Psi_{\mathrm{in}} = \lim_{t \to -\infty} \Psi_t,$$

exist in the strong topology of $\mathcal{H}$. The resulting vectors are independent of the representative fields used. The maps

$$\Omega_\pm : \mathcal{F}(\mathcal{H}_1) \to \mathcal{H}, \qquad \Omega_\pm(a^\dagger(f_1)\cdots a^\dagger(f_n)|0\rangle) = \Psi_{\text{in/out}},$$

are isometries that intertwine free and interacting translations. The scattering operator satisfies

$$S = \Omega_-^\dagger \Omega_+.$$

Sketch of proof.

1. *Velocity separation ⇒ commutator decay:* For large t, operators $A_i(t)$ become approximately spacelike separated, hence
$$\|[A_i(t), A_j(t)]\| \to 0 \qquad (i \neq j).$$
2. *Cook-type argument:* One shows the Cauchy property by bounding
$$\|\Psi_{t_2} - \Psi_{t_1}\| \leq \int_{t_1}^{t_2} ds \left\| \frac{d}{ds}\Psi_s \right\|,$$
and using the decay of commutators to prove integrability.
3. *Independence of field choice:* Off-shell contributions cancel in the $t \to \pm\infty$ limits.
4. *Fock-space structure:* Inner products factorize in the asymptotic limits, proving the isometry and Fock-space identification.

3. Cook–type integrability estimate

We show [22] that the family

$$\Psi_t \;=\; A_{f_1}(t)\, A_{f_2}(t) \cdots A_{f_n}(t)\, \Omega,$$
$$A_{f_j}(t) := \Phi(f_j, t)\, e^{+i\omega t}$$

is Cauchy in $\mathcal{H}$ when the wavepacket profiles f_j have pairwise disjoint *velocity supports*. The standard Cook argument reduces the existence of the strong limits $\Psi_{\text{out}} = \lim_{t\to+\infty} \Psi_t$ and $\Psi_{\text{in}} = \lim_{t\to-\infty} \Psi_t$ to an integrability bound on the time derivative $\dot\Psi_t \equiv d\Psi_t/dt$.

a. 1. Formal expression for the derivative. Differentiate Ψ_t with respect to t. Using the product rule and the definition $A_{f_j}(t) = \Phi(f_j, t)e^{i\omega t}$ we obtain

$$\frac{d}{dt}\Psi_t = \sum_{j=1}^{n} A_{f_1}(t) \cdots \dot A_{f_j}(t) \cdots A_{f_n}(t)\, \Omega, \tag{10}$$

with

$$\begin{aligned} \dot A_{f_j}(t) &= \big(\partial_t \Phi(f_j, t)\big) e^{i\omega t} + i\Phi(f_j, t)\, \omega\, e^{i\omega t} \\ &= i\,[H, \Phi(f_j, t)]\, e^{i\omega t} + i\Phi(f_j, t)\, \omega\, e^{i\omega t}, \end{aligned} \tag{11}$$

where we used the Heisenberg equation $\partial_t \Phi(f_j, t) = i[H, \Phi(f_j, t)]$.

Combine the two terms in (11) by introducing the operator

$$\begin{aligned} R_j(t) \;&:=\; \big(H - \omega\big)\, \Phi(f_j, t)\, e^{i\omega t} \\ &=\; \big([H, \Phi(f_j, t)] + \Phi(f_j, t)\, \omega\big) e^{i\omega t}. \end{aligned}$$

Thus

$$\dot A_{f_j}(t) \;=\; i\, R_j(t).$$

Substituting into (10) yields

$$\dot\Psi_t \;=\; i \sum_{j=1}^{n} A_{f_1}(t) \cdots R_j(t) \cdots A_{f_n}(t)\, \Omega. \tag{12}$$

b. 2. Use of the one–particle projection. Let P_1 denote the spectral projection onto the isolated one–particle subspace $\mathcal{H}_1$. Split $\Phi(f_j, t)$ into its on-shell (one–particle) and off-shell parts:

$$\begin{aligned} \Phi(f_j, t) \;&=\; P_1 \Phi(f_j, t) P_1 \;+\; \big(\Phi(f_j, t) - P_1 \Phi(f_j, t) P_1\big) \\ &=: \Phi_j^{(\text{on})}(t) + \Phi_j^{(\text{off})}(t) \end{aligned}$$

Acting on the vacuum, only the "on" part contributes to the leading one–particle creation:

$$\Phi_j^{(\text{on})}(t)\, \Omega = \Phi(f_j, t)\, \Omega,$$

$\Phi_j^{(\text{off})}(t)\, \Omega$ is small in a sense made precise below.

Observe that $(H - \omega)P_1 = 0$ on $\mathcal{H}_1$. Hence the leading contribution of $R_j(t)$ when $\Phi(f_j, t)$ is approximately on-shell is small: schematically

$$R_j(t) = (H - \omega)\big(\Phi_j^{(\text{off})}(t)\big) e^{i\omega t}$$

and thus $R_j(t)$ is dominated by the off-shell part of the smeared field.

c. 3. Norm estimate via commutator clustering. We estimate the norm of the generic summand in (12). Fix j and write

$$S_j(t) \;:=\; A_{f_1}(t) \cdots R_j(t) \cdots A_{f_n}(t)\, \Omega.$$

Move all factors with index $k < j$ to the left and those with $k > j$ to the right; successive commutations produce sums of nested commutators. By locality (and the velocity separation hypothesis) for large $|t|$ the supports of the wavepackets become spacelike separated so that commutators decay rapidly. Concretely, for each pair $i \neq j$ there exist constants $C_{N,ij}$ such that for any $N \in \mathbb{N}$

$$\big\|[A_{f_i}(t), A_{f_j}(t)]\big\| \leq C_{N,ij}\, (1 + |t|)^{-N}. \tag{13}$$

This follows from the fact that the spatial separation grows linearly in $|t|$ due to distinct group velocities and from standard propagation estimates combined with almost-locality of smeared fields. (One may choose N

arbitrarily large by increasing smoothness/decay of the test functions f_i.)

Using (13) and repeatedly commuting to cluster the operators around $R_j(t)\Omega$, one obtains the bound

$$\|S_j(t)\| \le \big\|R_j(t)\Omega\big\| + \sum_{\ell\ge 1} C'_{N,\ell}\,(1+|t|)^{-N_\ell},$$

where the correction terms (with constants $C'_{N,\ell}$) arise from nested commutators and can be made to decay faster than any polynomial by choosing sufficiently regular wavepackets. Thus it suffices to estimate $\|R_j(t)\Omega\|$.

d. 4. Estimate of the off–shell contribution. Recall $R_j(t) = (H-\omega)\Phi(f_j,t)e^{i\omega t}$. Acting on the vacuum we can insert the spectral resolution of H and use that the one–particle mass shell gives the on-shell delta-contribution which is annihilated by $(H-\omega)$. Therefore the dominant contribution to $R_j(t)\Omega$ comes from the off-shell spectral components. Using the spectral theorem and the rapid decay of the wavepacket's Fourier transform away from the mass shell one finds, for any integer $M \ge 1$, constants $C_{M,j}$ such that

$$\big\|R_j(t)\Omega\big\| \le C_{M,j}\,(1+|t|)^{-M}. \tag{14}$$

Intuitively, the factor $(H-\omega)$ produces an extra power of the off-shell energy which, when combined with the smooth, compactly supported momentum profile of f_j, yields arbitrarily fast decay in time after the phase oscillations are accounted for (Riemann–Lebesgue type estimate). A rigorous derivation follows from stationary phase estimates applied to the Fourier representation of $\Phi(f_j,t)\Omega$ and the separation of the mass shell (see standard expositions).

e. 5. Combine estimates to show integrability. Collecting the above bounds, for any $M \ge 1$ there exists C_M such that

$$\big\|\dot\Psi_t\big\| \le \sum_{j=1}^{n} \|S_j(t)\| \le C_M\,(1+|t|)^{-M}.$$

Choose $M \ge 2$ so that $(1+|t|)^{-M}$ is integrable on $[T,\infty)$ for any finite T. Then for $t_2 > t_1$,

$$\big\|\Psi_{t_2} - \Psi_{t_1}\big\| \le \int_{t_1}^{t_2} \big\|\dot\Psi_s\big\|\,ds \le C_M \int_{t_1}^{t_2} (1+|s|)^{-M} ds \to 0 \quad \text{as } t_1, t_2 \to \infty,$$

so $\{\Psi_t\}_{t\ge T}$ is Cauchy and hence convergent in norm. The identical argument for $t \to -\infty$ yields existence of the incoming limit.

G. Reduction of the one–particle, low–momentum sector to an effective Schrödinger operator

1. Lattice Hamiltonian. Consider the standard lattice scalar Hamiltonian on a one–dimensional spatial lattice with spacing a and sites labeled by integer n:

$$H \;=\; \sum_n \left[\frac{\Pi_n^2}{2} \;+\; \frac{(\phi_{n+1}-\phi_n)^2}{2a^2} \;+\; \frac{m_0^2}{2}\phi_n^2\right] \;+\; H_{\rm int}, \tag{15}$$

where ϕ_n, Π_n are canonical lattice field and conjugate momentum satisfying $[\phi_n, \Pi_m] = i\delta_{nm}$. $H_{\rm int}$ contains interaction terms (e.g. $\lambda\phi_n^4/4!$) and possibly an external/source term which we will denote explicitly later.

2. Mode expansion and diagonalization of the free part. Define discrete Fourier modes (periodic boundary conditions, N sites, lattice length $L = Na$):

$$\phi_n \;=\; \frac{1}{\sqrt{N}}\sum_k \tilde\phi_k\, e^{ikna}, \qquad \Pi_n \;=\; \frac{1}{\sqrt{N}}\sum_k \tilde\Pi_k\, e^{-ikna},$$

with $k = \frac{2\pi}{L}s$, $s \in \{-N/2, \dots, N/2-1\}$. The free (quadratic) part diagonalizes after the usual canonical transformation

$$\phi_n = \frac{1}{\sqrt{N}}\sum_k \frac{1}{\sqrt{2\omega_k}}\big(a_k e^{ikna} + a_k^\dagger e^{-ikna}\big), \tag{16}$$

$$\Pi_n = \frac{-i}{\sqrt{N}}\sum_k \sqrt{\frac{\omega_k}{2}}\big(a_k e^{ikna} - a_k^\dagger e^{-ikna}\big), \tag{17}$$

where the lattice dispersion is

$$\omega_k^2 \;=\; m_0^2 \;+\; \frac{4}{a^2}\sin^2\!\big(\tfrac{ka}{2}\big). \tag{18}$$

The free Hamiltonian becomes

$$H_{\rm free} \;=\; \sum_k \omega_k \Big(a_k^\dagger a_k + \tfrac{1}{2}\Big).$$

3. One–particle sector and continuum/low–momentum expansion. Single–particle states are created by $a_k^\dagger$ on the vacuum: $|k\rangle \equiv a_k^\dagger|0\rangle$ with energy ω_k. For low momenta $ka \ll 1$, expand ω_k in powers of k:

$$\omega_k = \sqrt{m_0^2 + k^2 + \mathcal{O}(k^4a^2)} \;=\; m + \frac{k^2}{2m} + \mathcal{O}(k^4),$$

where m denotes the renormalized (or tree-level in this free expansion) mass. (We denote by $m_{\rm eff}$ the physical effective mass after including self–energy renormalization from $H_{\rm int}$.) The important observation is that for small k,

$$\omega_k - m \approx \frac{k^2}{2m} \quad \text{(nonrelativistic dispersion)}.$$

Introduce lattice-position creation operators by inverse Fourier transform

$$a_x^\dagger \;:=\; \frac{1}{\sqrt{N}}\sum_k e^{-ikx}\, a_k^\dagger, \qquad x = na,$$

which create a particle localized (on the lattice) at site x. A general one–particle state is

$$|\psi\rangle \;=\; \sum_x \psi(x)\, a_x^\dagger|0\rangle, \qquad \sum_x |\psi(x)|^2 = 1.$$

Projecting $H_{\rm free}$ to the one–particle subspace (and subtracting the rest energy m) gives the nonrelativistic kinetic operator:

$$H_{\rm NR,kin} := \sum_k (\omega_k - m)\, a_k^\dagger a_k \approx \sum_k \frac{k^2}{2m}\, a_k^\dagger a_k \;=\; \sum_x a_x^\dagger \left(-\frac{1}{2m}\Delta_x\right) a_x, \quad (19)$$

where Δ_x is the discrete Laplacian on the lattice (in the continuum limit $\Delta_x \to \partial_x^2$). Thus, in the continuum/low–momentum limit,

$$H_{\rm NR,kin} \longrightarrow \int dx\; a_x^\dagger \left(-\frac{\partial_x^2}{2m}\right) a_x.$$

Acting on the one–particle wavefunction $\psi(x)$, this yields the familiar kinetic term $\frac{\hat{p}^2}{2m}\psi(x)$.

4. Emergence of a one–particle potential from external/background sources. To obtain a one–particle potential we introduce an external (classical) source or background that couples linearly to the field:

$$H_{\rm ext} \;=\; \sum_n J_n\, \phi_n,$$

with J_n a given (slowly varying, low–momentum) profile. Substitute the low–momentum mode expansion (16). In the long wavelength (small k) approximation $\omega_k \approx m$, so the field at site n is approximately

$$\phi_n \;\approx\; \frac{1}{\sqrt{2m}}\big(a_n + a_n^\dagger\big), \qquad a_n := a_{x=na}.$$

Hence

$$H_{\rm ext} \;\approx\; \sum_n J_n \,\frac{1}{\sqrt{2m}}\,(a_n + a_n^\dagger).$$

Project $H_{\rm ext}$ into the one–particle subspace: the only nonvanishing matrix elements between one–particle states come from terms of the form $a_n^\dagger a_n$ (generated when expanding products or from second–order effects). To see the direct potential term, compute the matrix element between position states:

$$\langle 0|a_x\, H_{\rm ext}\, a_{x'}^\dagger|0\rangle \;\approx\; \frac{1}{\sqrt{2m}} J_x\, \delta_{xx'}.$$

Thus to leading order the external source gives a diagonal (local) potential in the one–particle position basis:

$$V_{\rm eff}(x) \;=\; \frac{J_x}{\sqrt{2m}}$$

More generally, an external potential that couples to energy density or ϕ^2 will also project to an effective one–particle potential (with different prefactors). The precise coefficient depends on the normalization chosen for ϕ and on the on–shell residue Z if renormalization is included.

5. Interaction effects and mass renormalization. Terms in $H_{\rm int}$ which are nonlinear in ϕ (e.g. $\lambda\phi^4$) do not create one–particle → one–particle transitions at leading order except via loop (tadpole/self–energy) corrections. Their main effect in the one–particle sector is:

- a renormalization of the rest energy $m_0 \mapsto m_{\rm eff}$ (shift of the mass shell);
- small momentum dependent corrections to the dispersion ω_k (i.e. effective mass and higher derivative corrections giving e.g. $\mathcal{O}(k^4)$ terms);
- in the presence of inhomogeneous background expectation values $\langle\phi_n\rangle \neq 0$, a position–dependent one–particle potential arises from expanding interactions around that background (tadpole/backreaction).

Therefore after renormalization and projection to the one–particle sector we may write

$$H_{\rm 1p} \;=\; m_{\rm eff} + \sum_k (\omega_k - m_{\rm eff})\, a_k^\dagger a_k + \sum_x V_{\rm eff}(x)\, a_x^\dagger a_x + \cdots,$$

with $\omega_k - m_{\rm eff} \simeq k^2/(2m_{\rm eff})$ for small k.

6. Continuum limit and final effective Schrödinger operator. Going to the continuum position representation and restricting to low momenta, the one–particle Hamiltonian acting on the wavefunction $\psi(x)$ becomes

$$H_{\rm eff}\psi(x) \;=\; \Big(m_{\rm eff} \;-\; \frac{1}{2m_{\rm eff}}\frac{d^2}{dx^2} \;+\; V_{\rm eff}(x)\Big)\psi(x) + \mathcal{O}(\partial_x^4,\ \text{in.})$$

Subtracting the constant rest energy $m_{\rm eff}$ (which only contributes an overall phase in time evolution) yields the familiar nonrelativistic Schrödinger operator

$$\tilde{H}_{\rm eff} \;=\; -\frac{1}{2m_{\rm eff}}\frac{d^2}{dx^2} + V_{\rm eff}(x).$$

H. Connection to the Jordan–Lee–Preskill Discretized QFT

The JLP Hamiltonian for a discretized scalar field in $1+1$ dimensions,

$$H_{\rm JLP} = \sum_n \left[\frac{\Pi_n^2}{2} + \frac{(\phi_{n+1}-\phi_n)^2}{2a^2} + \frac{\lambda}{4!}\phi_n^4\right],$$

reduces [23] in the one-particle and fixed-parity sector to an effective Schrödinger operator

$$H_{\text{eff}} = \frac{p^2}{2m_{\text{eff}}} + V_{\text{eff}}(x),$$

matching the potentials studied in this work. Thus the scattering phase shifts and resonance widths extracted from our simulations reproduce the low-energy S–matrix of a discretized interacting QFT, consistent with Haag–Ruelle and LSZ.

VIII. ACKNOWLEDGEMENTS

We would like to thank Prof. Aninda Sinha and Ujjwal Basumatary for their wonderful course HE 381: Quantum Field theory on a quantum computer. The authors acknowledge use of Google Gemini for debugging code and improving the flow of the term paper. Creation of figures and understanding the material was a joint effort by both the authors.

[1] Soumyadeep Sarma, Jukka I. Väyrynen, and Elio J. König, "Design and benchmarks for emulating kondo dynamics on a quantum chip," Phys. Rev. B **111**, 235142 (2025).
[2] R. Landauer, "Spatial variation of currents and fields due to localized scatterers in metallic conduction," IBM Journal of Research and Development **1**, 223–231 (1957).
[3] João Barata and Enrique Rico, "Real-time simulation of jet energy loss and entropy production in high-energy scattering with matter," (2025), arXiv:2502.17558 [hep-ph].
[4] Isam Ben Soltane and Nicolas Bonod, "Extracting complete resonance characteristics from the phase of physical signals," (2025), arXiv:2412.10157 [physics.optics].
[5] Takashi Mori, "Floquet states in open quantum systems," Annual Review of Condensed Matter Physics **14**, 35–56 (2023).
[6] Luca D'Alessio Marin Bukov and Anatoli Polkovnikov, "Universal high-frequency behavior of periodically driven systems: from dynamical stabilization to Floquet engineering," Advances in Physics **64**, 139–226 (2015).
[7] R. Somma, G. Ortiz, J. E. Gubernatis, E. Knill, and R. Laflamme, "Simulating physical phenomena by quantum networks," Phys. Rev. A **65**, 042323 (2002).
[8] Alberto García-Vela, "Quantum control of resonance lifetimes in molecular photodissociation with intense laser fields," Journal of Chemical Theory and Computation **21**, 1547–1560 (2025).
[9] Ashutosh Singh, Pooja Siwach, and P. Arumugam, "Quantum simulations of nuclear resonances with variational methods," (2025), arXiv:2504.11685 [quant-ph].
[10] John Preskill, "Simulating quantum field theory with a quantum computer," PoS **LATTICE2018**, 024 (2018), arXiv:1811.10085 [hep-lat].
[11] Stephen P. Jordan, Keith S. M. Lee, and John Preskill, "Quantum computation of scattering in scalar quantum field theories," (2019), arXiv:1112.4833 [hep-th].
[12] David J. Griffiths and Darrell F. Schroeter, *Introduction to quantum mechanics*, third edition ed. (Cambridge University Press, Cambridge ; New York, NY, 2018).
[13] Philip M Morse, "Diatomic molecules according to the wave mechanics. ii. vibrational levels," Physical review **34**, 57 (1929).
[14] G. Rawitscher, Cory Merow, Matthew Nguyen, and Ionel Simbotin, "Resonances and quantum scattering for the morse potential as a barrier," American Journal of Physics **70**, 935–944 (2002), https://pubs.aip.org/aapt/ajp/article-pdf/70/9/935/7530254/935$_1$o*nline.pdf*.
[15] J. J. Sakurai and Jim Napolitano, *Modern Quantum Mechanics*, 3rd ed. (Cambridge University Press, Cambridge, 2020).
[16] Dorit Aharonov, Vaughan Jones, and Zeph Landau, "A polynomial quantum algorithm for approximating the jones polynomial," Algorithmica **55**, 395–421 (2009).
[17] Michael Reed and Barry Simon, *Methods of Modern Mathematical Physics III: Scattering Theory* (Academic Press, 1979).
[18] Dmitri Yafaev, "Lectures on scattering theory," (2004), arXiv:math/0403213 [math.SP].
[19] K. Ito and E. Skibsted, "Scattering theory for c^2 long-range potentials," (2024), arXiv:2408.02979 [math-ph].
[20] John Collins, "A new approach to the lsz reduction formula," (2019), arXiv:1904.10923 [hep-ph].
[21] K. Hepp, "On the connection between the lsz and wightman quantum field theory," Communications in Mathematical Physics **1**, 95–111 (1965).
[22] J. M. Cook, "Convergence to the møller wave-matrix," Journal of Mathematics and Physics **36**, 82–87 (1957), original statement of Cook's criterion for existence of Møller (wave) operators.
[23] R. Haag and D. Ruelle, "On the asymptotic condition in quantum field theory," Physical Review **112**, 669–670 (1958).